Electronic Supporting Information (ESI)

Bidirectional strain release in a thermosalient organic salt crystal induced by Anisotropic thermal expansion and phase transformation

Priyasha Harsha [a] *and Dinabandhu Das*[*a]

School of Physical Sciences, Jawaharlal Nehru University, New Delhi-110067, India

Email: jnu.dinu@gmail.com

Contents

1. List of thermosalient crystals studied till date

Table S1 List of thermosalient crystals

Sl. No.	Name of Compound	Mechanism	References
1.	(phenylazophenyl)palladium hexafluoroacetylacetonate (PHA)	Phase Transformation	*J. Am. Chem. Soc*. 1983, **105**, 641–643; *RSC Adv.*, 2014,**4**, 7640-7647; *Nat. Commun.*, 2014, **5**, 4811.
2.	hexadecahydropyrene	Phase Transformation	*Acta Cryst*.,1991**, B47,** 739-742
3.	(±)-3,4-di-O-acetyl-1,2,5,6-tetra-O-benzyl-myo-inositol	Phase Transformation	*Acta Cryst*.,1993**, B49,** 708-718
4.	Oxitropium Bromide	Phase Transformation	*Acta Cryst.Sect. A*, 1991, **49**, c436**;** *J. Am. Chem. Soc.* 2010, **132**, 14191–14202
5.	4,5-Bis(fluorodinitromethyl)-2-methoxy-1,3-dioxolane	Molecular Twisting	*Acta Cryst.*,1996, C**52**, 1851-1853
6.	$NiCr_2O_4$ and $CuCr_2O_4$	Phase Transformation	*J. Mater. Chem.*, 1997**, 7**, 143-146
7.	$[3_6]$(1,2,3,4,5,6)cyclophane	Phase Transformation	Tetrahedron Lett., 2000, **41,** 7933-7938
8.	Pentacene	Phase Transformation	*Adv. Mater.*, 2007, **19,** 2079
9.	N-2-propylidene-4-hydroxybenzohydrazide	Phase Transformation	*CrystEngComm,* 2014, **14**, 2645–2653
10.	1,2,4,5-Tetrabromobenzene	Phase Transformation	*Chem. Mater.* 2000, **12**, 490– 494 *J. Am. Chem. Soc.,* 2013**, 135,** 13843–13850
11.	$[ZnBr_2(2,2'\text{-bipy})]$	Phase Transformation	*Chem. Commun.*, 2013,**49**, 9293-9295
12.	L- PGA and D- PGA (PGA= pyroglutamic acid).	Phase Transformation	*J. Am. Chem. Soc.*, 2015, **137**,1895–1902
13.	2,6-Dichlorobenzylidene-4-fluoro-3-nitroaniline	Phase Transformation	*J. Am. Chem. Soc.,* 2015, **137**, 9912–9921
14.	Nitromethane solvate of 18-crown-6	Anisotropic Thermal Expansion	*Chem. Mater.* 2016, **28,** 5073–5079
15.	solid solutions of [Zn(2,2'-bpy)Br2] with [Zn(2,2'-bpy)Cl2] and [Zn(2,2'-bpy)BrCl]	Phase Transformation	*CrystEngComm*, 2016**,18,** 4699-4703
16.	Alkylacridones and Their Dicyanomethylene Derivatives	Anisotropic Thermal Expansion	*Chem. Eur. J.* 2016, **22,** 7763 – 7770

17.	N′-2-propylydene-4-hydroxybenzohydrazide,an imine of acetone (IMACET)	Anisotropic Thermal Expansion	*Sci Rep.,* 2016, **6**, 29610; *Cryst. Growth Des.* 2017, **17**, 4445−4453
18.	[Fe(5-Br-salEen)$_2$][ClO_4] (salEen= *N*-ethyl-*N*-(2-aminoethyl)salicylaldiminate)	Phase Transformation	*Chem. Sci.*, 2016,**7**, 4251-4258
19.	4-((3,5-dichloro-2-hydroxybenzylidene)amino)benzamide	Phase Transformation	*IUCrJ,* 2017, **4**, 243–250
20.	Azomethine–Boron Complex	Phase Transformation	*Chem. Eur. J.* 2017, 23, 11827 – 11833
21.	Pyrene tweezers	Phase Transformation	*Chem. Asian J.* 2017, **12**, 811 – 815
22.	3,5-Dichlorosalinazid and 3,5-Dibromo-salinazid 3-bromo-5-chloro-salinazid	Phase Transformation	*IUCrJ*, 2017, **4**, 812–823
23.	Pseudorotaxanes complexes: (i) [ferrocenylmethyl(4-methylphenyl)ammonium·DB24C8]+(PF6)− rotaxane. [ruthenocenylmethyl(4-methylphenyl)ammonium·DB24C8]+(PF6)− rotaxane	Phase Transformation	*Sci Rep.,* 2017, **7**,14195
24.	Methscopolamine Bromide	Anisotropic thermal expansion	*Crystals,* 2018, ***8***, 301
25.	CNB-BPY and Slz-PFB salinazide (Slz), 3-chloro-2-nitrobenzoic acid (CNB), pentafluorobenzoic acid (PNB) 4,4′-bipyridine (BPY),	Phase Transformation	*Cryst. Growth Des.* 2018, **18,** 2918–2923
26.	*N*,*N*′-dipropylated diketopyrrolopyrrole	Phase Transformation	*CrystEngComm*, 2018, **20**, 5317-5320
27.	Naphthalene-2,3-diyl-bis(4-halogenobenzoate)s 2 (X = F) and 3 (X = Cl)cr	Phase Transformation	*Chem. Eur. J.* 2018, **24**, 4133 – 4139
28.	[Fe(5-I-salEen)$_2$]ClO_4	Phase Transformation	*Eur. J. Inorg. Chem.* 2018, 2976–2983
29.	Alkoxyphenyl *N*-substituted NDIs (ANDIs)	Phase Transformation	*CrystEngComm*, 2018,**20**, 6054-6060
30.	4-Aminobenzonitrile	Phase Transformation	*Chem. Commun.*, 2018,**54**, 6208-6211
31.	3-((4-chlorophenyl)imino)indolin-2-one,	Phase Transformation	*Cryst. Growth Des.* 2018, **18,** 3927–3937
32.	Pyrene and 1,8-Dinitroanthraquinone	Phase Transformation	*Cryst. Growth Des.* 2018, **18**, 6670–6680
33.	Tetrahydrate berberine chloride	Phase Transformation	*CrystEngComm*, 2018, **20**, 2253-2257

34.	Terepthalic acid	Phase Transformation	*Nat Commun,* **2019,** 10, 3723.
35.	Bis-,Tri-,and Tetraphenylethene	Phase Transformation	*Chemistry Lett*, 2020, **49,** 174–177
36.	Cocrystal of Carbazole and DABCO	Phase Transformation	*Matter*, 2019, **1**, 1033–1046.
37.	triphenylethenyl gold 4-chlorophenyl isocyanide complex	Phase Transformation	*Chem. Sci.*, 2019,**10**, 4185-4191
38.	2,2′-((1E,1′E)-(((Z)-ethene-1,2-diyl)bis(azaneylylidene))bis(ethan-1-yl-1-ylidene))diphenolate cobalt(II) hemisolvate (**[CoL]·0.5. MeOH**)	Phase Transformation	*Chem. Lett.*, 2019, **48,** 1077-1080.
39.	hydrogen-bonded organic framework (HOF) of tetra[2,3]thienylene tetracarboxylic acid	Molecular rotation and desolvation	*Angew. Chem. Int. Ed.,* 2019, **58,** 10345–10352
40.	tapentadol hydrochloride	Phase Transformation	*Acta Cryst.,* 2019, **B75**, 183-191
41.	4-diethynyl-2,3-difluorophenylene rotator linked to two gold(I) nodes	Anisotropic Thermal Expansion	*Angew. Chem. Int. Ed.,* 2019, **58,** 18003-18010.
42.	2,7-di([1,1′-biphenyl]-4-yl)-fluorenone molecules **(4-DBpFO)**	Phase Transformation	*Nat. Commun*. 2019, **10**, 4573.
43.	dl-norleucine	Phase Transformation	*IUCrJ*, 2020, **7**, 331–341
44.	Charge-transfer (CT) complex 3,3′,5,5′-tetramethylbendizine-7,7,8,8-tetracyanoquinodimethane	Phase Transformations	*Cryst. Growth Des.* 2020, **20**,4758–4763.
45.	Disilanyl macrocycle C4 composed of four disilane (Si–Si) bonds and four p-phenylenes	Phase Transformation	*J. Am. Chem. Soc.* 2020, 142, 12651–12657
46.	2-[(anthracen-9-yl)methylidene]-2,3-dihydro-1-benzothiophen-3-one **(HTI-An)**	Phase Transformation	*J. Mater. Chem. C*, 2021,**9**, 6789-6795.
47.	3,6-bis(4-chlorophenyl)-2-propyl-2,5-dihydropyrrolo[3,4-c]pyrrole-1,4-dione	Phase Transformation	*CrystEngComm*, 2021, **23**, 5882-5890
48.	1,2,4,5-tetrachlorobenzene	Phase Transformation	*Isr. J. Chem.* 2021, **61**, 1–7
49.	Coronene	Phase Transformation	*Sci Rep* 2021, **11**, 3175
50.	Naphthalene diimide Alkoxybenzyl system	Anisotropic thermal expansion	*J.Am.Chem.Soc*., 2021, **143**, 5951−5957
51.	(9-Isocyanoanthracene)gold(I) Complexes	Anisotropic thermal contraction	*Inorg. Chem.* 2021, **60,** 10849–10856

52.	α- 2-hydroxy-3,5-dibromobenzylidine-4-fluoro-3-nitroaniline	Phase Transformation	*Cryst. Growth Des.* 2022, **22,** 615–624
53.	5-Fluorobenzoyl-4-(4-methoxyphenyl)ethynyl-1-methylimidazole	Anisotropic thermal expansion	*Cryst. Growth Des.* 2022, **22**, 5904–5911
54.	Nickel(II) diisopropyldithiocarbamate	Phase Transformation	*Cryst. Growth Des.* 2022, **22**, 1951–1959
55.	$[Fe(L^{Ph,Et})_2(NCS)_2]$ ($L^{Ph,Et}$ = 1-phenyl-1*H*-1,2,3-triazole-4-yl-methylideneaminoethyl)	Phase Transformation	*CrystEngComm*, 2022,**24**, 4224-4234
56.	Naphthalidenimine–boron complexes	Phase Transformation	*ACS Appl. Mater. Interfaces* 2022, 14, 19, 22650–22657
57.	zinc(II) tetraphenylporphyrin	Phase Transformation	T. Sasaki, *BCSJ*, 2022, 95, 968–971
58.	Guanidinium nitrate	Phase Transformation	*Nat Comm*, 2022, 13, 2823
59.	(a) **TMP-25HBA** (TMP: Trimethoprim; 25HBA: 2,5-dihydroxybenzoic acid) (b) **TMP-OA** (TMP: Trimethoprim; OA: Orotic acid)	(a) Conformational changes (b) Phase Transformation	*Crystals,* 2023, **13**, 701.
60.	naphthalene diimide and tetrachlorocobaltate organic–inorganic hybrid metal halide (**OIMH**)	Removal of water molecules	*Dalton Trans.*, 2023, **52**, 10531-10536
61.	(2Z,2′Z)-2,2′-(1,4-phenylene)bis(3-(4-bromophenyl)acrylonitrile) (**DSBr**)	Uniaxial thermal expansion	*J. Mater. Chem. C*, 2024, **12**, 2515-2525
62.	L-asparagine (L-Asn) and d-asparagine (d-Asn)	Desolvation (Jumping mate strategy)	*J. Am. Chem. Soc.* 2024**, 146,** 9679–9687
63.	N-methyl-N-octylamino-substituted anthracene-pentiptycene π-system	Phase Transformation	*J. Am. Chem. Soc.* 2024, **146,** 8131–8141
64.	Anthracene-9-thiocarboxamide	Anisotropic Thermal Expansion	*Chem. Commun.,* 2024, **60**, 7697-7700
65.	(*E*)-4-chloro-*N*′-(4-(trifluoromethoxy)benzylidene)benzohydrazide **(CTBB)**	Phase Transformation	*Chem. Sci.,* 2024, **15**, 9287-9297
66.	Benzodifuranone	Phase Transformation	*Chem. Eur. J.,* 2024, e202402622.
67.	piperazinium trifluoroacetate salt (**PZTFA**)	Release of gas	*Small* **2024**, 2401317.

2. Experimental Section

- **Synthesis of SQIM salt.**

All the chemicals were purchased from Sigma-Aldrich and used without further purification. Methanol solvent is commercially available and was used after distillation. **SQIM** was prepared using the reported method.[1] 1:1 stoichiometric ration of, 11.4 mg (0.1 mmol) **SQ** and 6.8 mg (0.1 mmol) **IM** were ground together using a pestle and mortar. A small amount of methanol was added to facilitate liquid-assisted grinding (LAG) for 1 hour. The resulting powder was then dissolved in a 1:1 stoichiometric ratio of methanol and water for crystallisation. Colourless block-shaped single crystals were obtained through slow evaporation after two weeks. The synthesized compounds were characterized by FT- IR and Powder X-ray Diffraction.

a) FT-IR Spectra

Transmission infrared spectra of the solids were obtained using a Fourier–transform infrared spectrometer (Shimadzu), 43 scans were collected at 4 cm^{-1} resolution for each sample. The spectra were measured over the range of 4000-400 cm^{-1}.

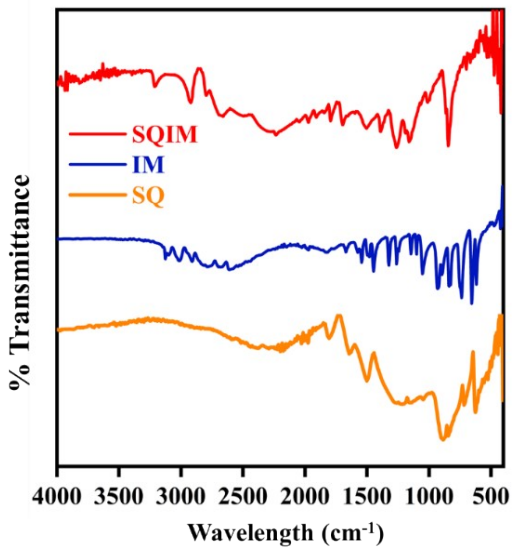

Figure S1 FT-IR Spectra of **SQIM, SQ and IM.**

3. Powder X-ray Diffraction Pattern

Powder X-ray diffractogram was measured on Rigaku powder X-ray diffractometer (Miniflex600 with Cu Kα radiation, λ = 1.54059 Å) operating in Bragg−Brentano geometry.

Crystals of the compound was crushed gently and layered on a sample holder. Data was recorded at room temperature at a scan rate of 2°/min from 5° to 40° (2θ value).

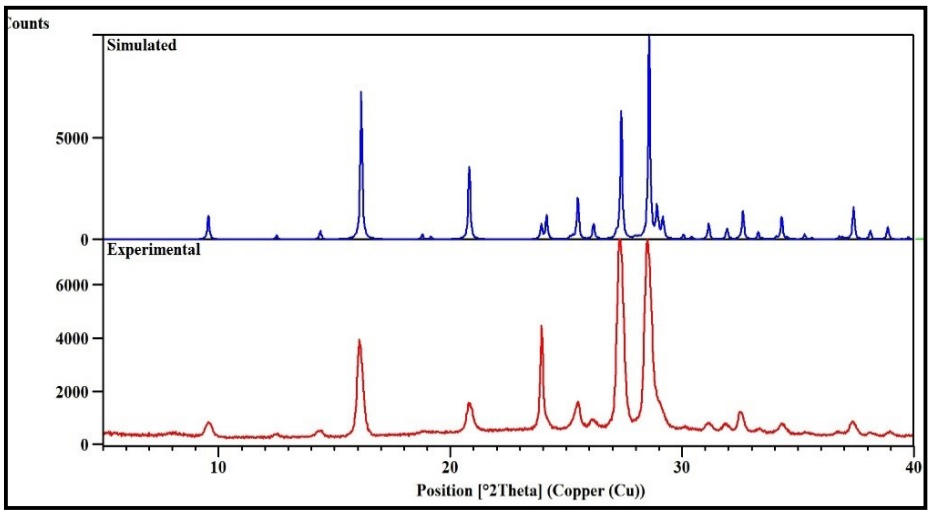

Figure S2. Simulated and experimental PXRD patterns of bulk sample of **SQIM** at room temperature.

4. Thermo-gravimetric analysis (TGA)

The TGA measurement of **SQIM** was performed on Mettler Toledo equipped with Minichiller MT/230 from 298K to 673K under nitrogen atmosphere (flow rate:20 ml /min and at a scan rate of 5 K / min.), using a software STARe version 13.00.

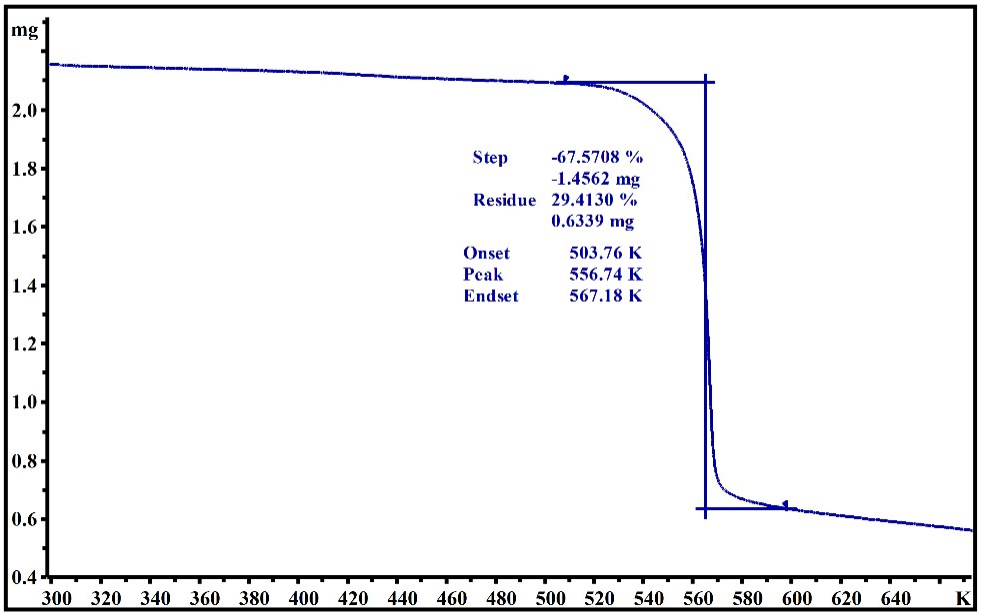

Figure S3. TGA of **SQIM.**

5. Differential Scanning Calorimetry

Differential scanning calorimetry (DSC) to observe the thermosalient behavior of **SQIM** at elevated temperatures was conducted using a Mettler Toledo DSC1 calorimeter equipped with

an FRS5 DSC sensor, along with a HUBER TC100-MT chiller and STARe software (v13.00). For the measurements, 2-4 mg of the sample was placed in an aluminium pan and sealed with a lid. During the experiment, the sample was purged with dry nitrogen gas at a flow rate of 20 mL/min, and the heating rate was set to 5 K/min. Low-temperature DSC (in main manuscript) analysis was performed at SAIF, IIT Bombay, using a Hitachi DSC calorimeter. In this experiment, 2-3 mg of the compound was used, with 20 mL/min flow rate of dry nitrogen gas and a cooling rate of 10 K/min.

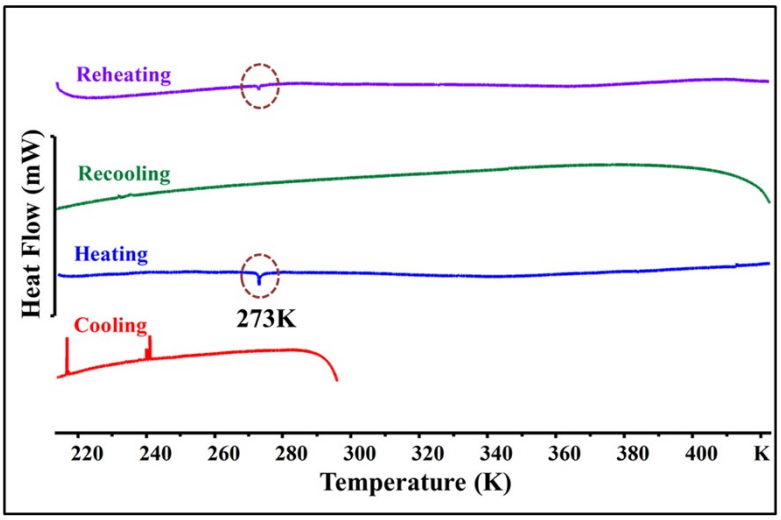

(a)

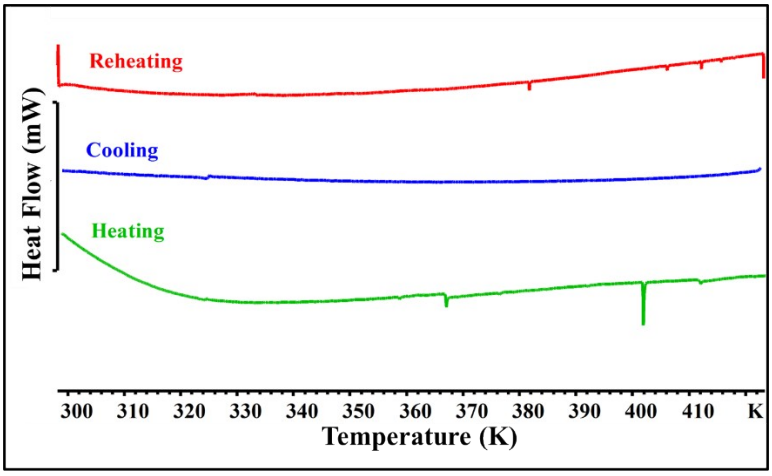

Figure S4. (a) DSC thermogram of **SQIM** showing irreversibility of the TS phenomenon but reversible phase transition occurs at 273K. (b) At higher temperatures crystals exhibit jumping only during heating

6. Cold and Hot Stage setups

In-house hot and cold stage setups were made for controlled heating or cooling experiments based on DSC observations to visualize the phenomenon.

To study the behavior of crystals at low temperatures, they were placed in a beaker submerged in a methanol bath. The bath was connected to an immersion cooler, capable of lowering the

temperature. The beaker was secured in the methanol bath using a metallic clamp, while the bath itself was connected to a metallic coil and temperature sensors. When the power supply was activated, the methanol in the bath cooled down to 193K. The movement of the crystals was recorded using a camera, which was attached to a clamp.

(a) **(b)**

Figure S5. (a) Cold stage setup to observe the jumping at low temperature. (b) Beaker immersed in the methanol bath, Crystals which come outside of the beaker after jumping (Red circle)**.**

To observe the behavior of crystals at elevated temperatures, crystals were placed on a petri dish and subjected to controlled heating using a Tarson hot plate. As we switched on the hot plate, the temperature gradually increased, creating a controlled environment for the crystals. A camera, securely attached to a clamp, continuously recorded the crystal's movements and any observed jumping behavior during the heating process. This setup allowed for a detailed examination of the crystals' response to rising temperatures.

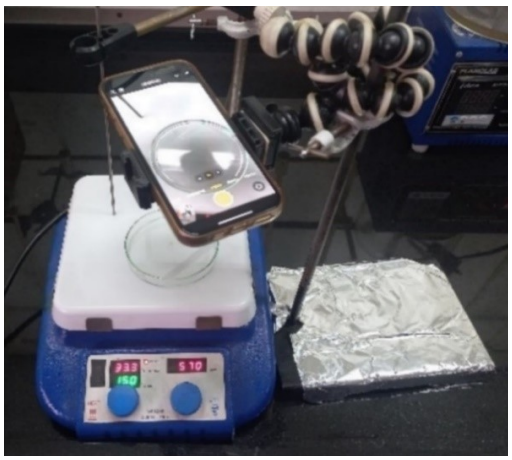

Figure S6. Hot stage setup to observe jumping at high temperature.

7. Single crystal X-Ray Diffraction

All the Single Crystal X-ray Diffraction experiments were performed in a Bruker D8 Quest single crystal X-ray diffractometer equipped with a microfocus anode (MoKα) and a PHOTON 100 CMOS detector. The integration and scaling of data were performed using the SAINT programs.[2] All the structures were solved by direct methods and refined by full-matrix least-square on F2 using SHELX-2019.[3] All non-hydrogen atoms were refined anisotropically. All the aromatic hydrogen atoms were placed using calculated positions on riding models. Positions of the hydrogen atoms on nitrogen atoms and the hydroxyl group were assigned using the Difference Fourier map. Temperature was controlled by Oxford Cryostream 800 Plus cryostat during VT-SCXRD experiments.

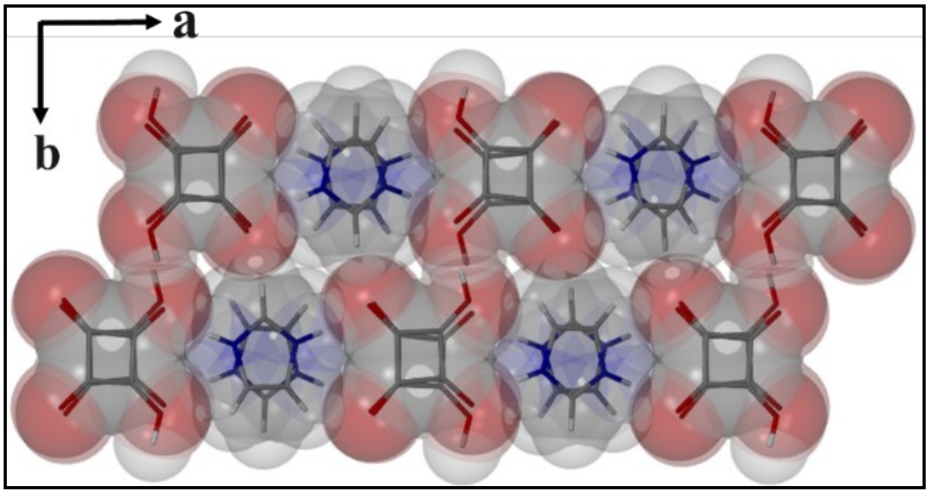

(a)

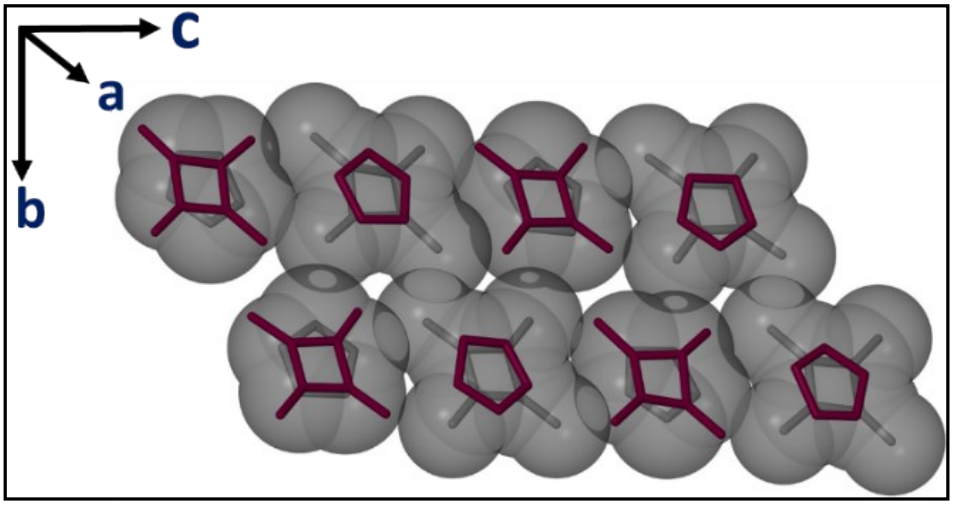

(b)

Figure S7. Stacked 2D layers in the crystal structure of **SQIM** at (a) 190K and (b) 150K.

a) Photographs of SQIM in VTSCXRD experiment

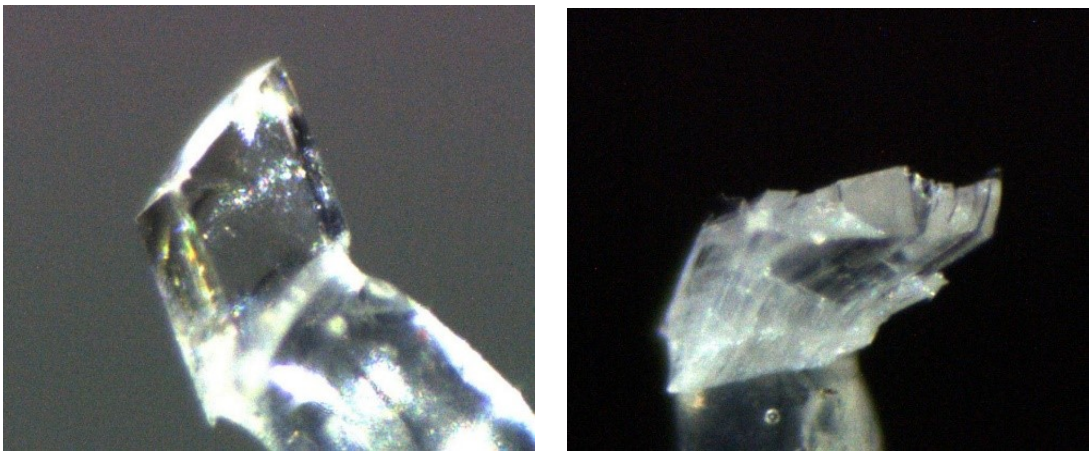

(a) **(b)**

Figure S8. Micrographic picture of **SQIM** at (a) 300K during VTSCXRD experiment from 300K to 190K; (b) Micrographic picture of **SQIM** taken at 150K.

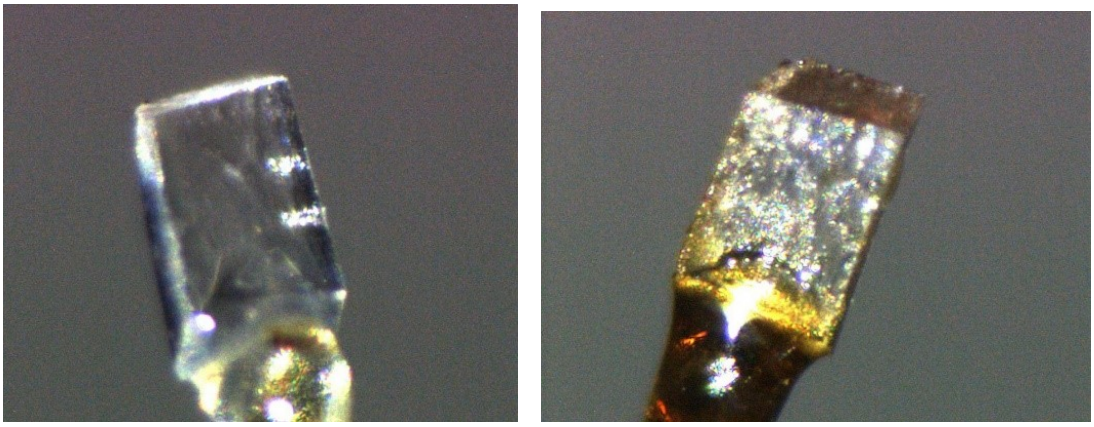

(c) **(d)**

Figure S9: Micrographic picture of **SQIM** (a) 250K (b) 450K during VTSCXRD experiment from 250K to 450K

b) Crystallographic Information

Table S2 Crystallographic parameters parameters of **SQIM** crystal structures determined by VTSCXRD from the temperature range 190K to 300K (Phase-I).

Identification code	**SQIM190K_LT**	**SQIM250K_LT**	**SQIM300K_LT**
Moiety formula	$C_7H_6N_2O_4$	$C_7H_6N_2O_4$	$C_7H_6N_2O_4$
Crystal system	Monoclinic	Monoclinic	Monoclinic
Space group	$P2_1/c$	$P2_1/c$	$P2_1/c$
a/Å	9.4038(10)	9.4072(10)	9.4094(10)
b/Å	10.9694(13)	10.9721(13)	10.9728(12)
c/Å	7.4547(10)	7.5088(10)	7.5549(10)

α/(°)	90	90	90
β/(°)	100.726(4)	100.453(4)	100.201(4)
γ/(°)	90	90	90
V/Å^3	755.55(16)	762.17(16)	767.69(16)
Z	4	4	4
D_{cal}/g cm^{-3}	1.601	1.587	1.576
T/K	190 (2)	250 (2)	300 (2)
μ/mm^{-1}	0.134	0.133	0.132
F_{000}	376	376	376
Reflection measured	13058	13107	13205
Unique reflections	1863	1877	1885
Observed reflections	1741	1741	1721
Parameters	142	142	142
R_{int}	0.0215	0.0200	0.0209
final R (I>2σ(I))	0.0342	0.0360	0.0383
final R(all data)	0.0362	0.0382	0.0413
GOF on F^2	1.096	1.081	1.078
CCDC No.	2383780	2383782	2383781

Table S3 Crystallographic data of crystals and structure refinement parameters of **SQIM** from the temperature range 250K to 450K (Phase-I).

Identification code	**SQIM250K_HT**	**SQIM300K_HT**	**SQIM350K_HT**	**SQIM400K_HT**	**SQIM450K_HT**
Moiety formula	$C_7H_6N_2O_4$	$C_7H_6N_2O_4$	$C_7H_6N_2O_4$	$C_7H_6N_2O_4$	$C_7H_6N_2O_4$
Crystal system	Monoclinic	Monoclinic	Monoclinic	Monoclinic	Monoclinic
Space group	$P2_1/c$	$P2_1/c$	$P2_1/c$	$P2_1/c$	$P2_1/c$
a/Å	9.3773(10)	9.3808(10)	9.3883(10)	9.4017(11)	9.4263(12)
b/Å	10.9848(13)	10.9778(13)	10.9737(14)	10.9631(15)	10.9519(16)
c/Å	7.5143(8)	7.5597(8)	7.6099(9)	7.6527(9)	7.6960(10)
α/(°)	90	90	90	90	90
β/(°)	100.458(4)	100.221(4)	99.955(4)	99.639(5)	99.340(5)
γ/(°)	90	90	90	90	90
V/Å^3	761.17(15)	766.15(15)	772.20(16)	777.642(17)	784.15(18)
Z	4	4	4	4	4
D_{cal}/g cm^{-3}	1.589	1.579	1.567	1.556	1.543
T/K	250 (2)	300 (2)	350 (2)	400 (2)	450 (2)
μ/mm^{-1}	0.133	0.132	0.131	0.130	0.129
F_{000}	376	376	376	376	376

Reflection measured	13599	13719	13912	14013	14230
Unique reflections	1880	1890	1912	1925	1943
Observed reflections	1738	1703	1652	1602	1484
Parameters	142	142	142	142	142
R_{int}	0.0201	0.0213	0.0224	0.0223	0.0254
final R (I>2σ(I))	0.0361	0.0380	0.0409	0.0461	0.0579
final R(all data)	0.0387	0.0422	0.0466	0.0539	0.0708
GOF on F^2	1.064	1.058	1.073	1.070	1.097
CCDC No.	2383785	2383786	2383787	2383788	2383789

Table S4 Crystallographic parameters of **Phase-II** structure of **SQIM** determined at 150K

Identification code	**SQIM150K_LT (Phase-II)**
Moiety formula	$C_7H_6N_2O_4$
Crystal system	Monoclinic
Space group	$P2_1/c$
a/Å	7.264(4)
b/Å	21.365(11)
c/Å	9.973(5)
α/(°)	90
β/(°)	100.19(2)
γ/(°)	90
V/Å^3	1523.35
Z	8
D_{cal}/g cm^{-3}	1.588
T/K	150 (2)
μ/mm^{-1}	0.133
F_{000}	752
Reflection measured	5722
Unique reflections	2709
Observed reflections	1175
Parameters	243
R_{int}	0.0887
final R (I>2σ(I))	0.1627
final R(all data)	0.2746
GOF on F^2	1.385
CCDC No.	2383893

c) Hydrogen Bonding Parameters

Table S5 Hydrogen bonding parameters of **SQIM** from 190K to 300K (Phase-I)

H-bonding parameters		SQIM190K_LT	SQIM250K_LT	SQIM300K_LT
N1 H1•••O3	D H (Å)	0.89(2)	0.90(2)	0.914(2)
	H•••A (Å)	1.87(2)	1.87(2)	1.858(2)
	D•••A (Å)	2.760(1)	2.764(1)	2.769(1)
	∠D H•••A(˚)	173.83(1)	173.84(2)	174.84(2)
N2 H2•••O1	D H (Å)	0.89(2)	0.91(2)	0.921(2)
	H•••A (Å)	1.88(2)	1.87(2)	1.87(2)
	D•••A (Å)	2.774(1)	2.777(1)	2.781(1)
	∠D-H•••A (˚)	173.97(2)	173.44(2)	171.95(2)
O4 H4•••O1	D-H (Å)	0.95(2)	0.96(2)	0.97(2)
	H•••A (Å)	1.61(2)	1.60(2)	1.59(2)
	D•••A (Å)	2.547(1)	2.549(1)	2.549(1)
	∠D-H•••A(˚)	171.84(2)	171.27(2)	171.21(2)
C5 H5•••O2	D-H (Å)	0.93(2)	0.92(2)	0.92(2)
	H•••A (Å)	2.50(2)	2.51(2)	2.50(2)
	D•••A (Å)	3.219(1)	3.223(2)	3.227(2)
	∠D-H•••A(˚)	134.27(1)	13.80(1)	135.82(1)
C6 H6•••O4	D-H (Å)	0.92(2)	0.92(2)	0.90(2)
	H•••A (Å)	2.67(2)	2.67(2)	2.68(2)
	D•••A (Å)	3.324(1)	3.326(2)	3.329(2)
	∠D-H•••A (˚)	128.67(1)	128.73(1)	130.01(1)
C6 H6•••O2	D-H (Å)	0.92(2)	0.92(2)	0.90(2)
	H•••A (Å)	2.43(1)	2.45(2)	2.48(2)
	D•••A (Å)	3.194(1)	3.204(1)	3.215(2)
	∠D-H•••A (˚)	140.09(1)	139.07(1)	138.42(1)
C7 H7•••O3	D-H (Å)	0.95(2)	0.95(2)	0.96(2)
	H•••A (Å)	2.32(2)	2.31(2)	2.31(2)
	D•••A (Å)	3.124(1)	3.123(1)	3.123(2)
	∠D-H•••A (˚)	141.73(1)	142.67(1)	141.29(1)

NOTE: All the values are calculated from Platon software[4]

Table S6 Hydrogen bonding parameters of **SQIM** from 250K to 450K (Phase-I).

H-bonding parameters		**SQIM250K_HT**	**SQIM300K_HT**	**SQIM350K_HT**	**SQIM400K_HT**	**SQIM450K_HT**
N1 H1•••O3	D-H (Å)	0.90(2)	0.90(2)	0.90(2)	0.93(2)	0.97(3)
	H•••A (Å)	1.86(2)	1.87(2)	1.87(2)	1.86(2)	1.84(3)
	D•••A (Å)	2.759(1)	2.764(1)	2.773(2)	2.786(2)	2.805(2)
	∠D-H•••A(˚)	175.18(2)	175.04(2)	175.19(2)	175.75(2)	173.72(3)
N2 H2•••O1	D-H (Å)	0.91(2)	0.91(2)	0.93(2)	0.95(3)	1.01(3)
	H•••A (Å)	1.86(2)	1.87(2)	1.87(2)	1.86(3)	2.822(2)
	D•••A (Å)	2.772(1)	2.775(1)	2.785(2)	2.799(2)	2.822(2)
	∠D-H•••A (˚)	172.92(2)	172.60(2)	172.40(2)	170.26(2)	166.97(3)
O4 H4•••O1	D-H (Å)	0.96(2)	0.96(2)	0.97(2)	0.96(2)	0.97(2)
	H•••A (Å)	1.60(2)	1.59(2)	1.59(2)	1.59(2)	1.57(2)
	D•••A (Å)	2.551(1)	2.551(1)	2.548(1)	2.543(1)	2.534(2)
	∠D-H•••A(˚)	171.22(2)	171.56(2)	171.48(2)	170.44(2)	169.42(2)
C5 H5•••O2	D-H (Å)	0.92(2)	0.91(2)	0.90(2)	0.89(2)	0.86(3)
	H•••A (Å)	2.50(2)	2.51(2)	2.52(2)	2.51(2)	2.51(3)
	D•••A (Å)	3.218(2)	3.221(2)	3.222(2)	3.222(2)	3.217(3)
	∠D-H•••A(˚)	134.84(1)	135.11(1)	134.94(1)	136.58(2)	139.76(2)
C6 H6•••O4	D-H (Å)	0.92(2)	0.90(2)	0.90(2)	0.88(2)	0.83(3)
	H•••A (Å)	2.67(2)	2.67(2)	2.68(2)	2.70(2)	2.74(3)
	D•••A (Å)	3.320(2)	3.323(2)	3.327(2)	3.330(2)	3.333(3)
	∠D-H•••A (˚)	128.93(1)	129.80(1)	129.68(1)	129.11(2)	130.57(3)
C6 H6•••O2	D-H (Å)	0.92(2)	0.90(2)	0.90(2)	0.88(2)	0.83(3)
	H•••A (Å)	2.46(2)	2.48(2)	2.50(2)	2.52(2)	2.57(3)
	D•••A (Å)	3.209(1)	3.218(2)	3.228(2)	3.236(2)	3.240(3)
	∠D-H•••A (˚)	139.15(1)	139.12(1)	138.42(2)	138.39(2)	139.82(3)
C7 H7•••O3	D-H (Å)	0.95(2)	0.95(2)	0.96(2)	0.98(3)	1.02(4)
	H•••A (Å)	2.32(2)	2.32(2)	2.30(2)	2.29(3)	2.22(4)
	D•••A (Å)	3.126(1)	3.125(2)	3.122(2)	3.119(2)	3.112(3)
	∠D-H•••A (˚)	142.40(1)	142.06(1)	142.57(2)	141.90(2)	145.80(3)

NOTE: All the values are calculated from Platon software[4]

Table S7 Hydrogen bonding parameters of the crystal structure of **SQIM for phase-II** at 150K

	D-H (Å)	**H•••A (Å)**	**D•••A (Å)**	**∠D-H•••A (°)**
N1 H1A•••O7	0.861	1.916	2.770(8)	171.15
N2 H2A•••O5	0.860	1.903	2.760(9)	174.04
N3 H3A•••O4	0.860	1.909	2.768(8)	176.28
N4 H4A•••O2	0.860	1.878	2.730(8)	171.06
C9 H9•••O3	0.930	2.327	3.146(11)	146.55
C10 H10•••O6	0.930	2.528	3.171(10)	126.62
C11 H11•••O4	0.930	2.238	3.085(12)	150.91
C12 H12•••O5	0.930	2.270	3.115(12)	150.73
C13 H13•••O6	0.930	2.287	3.144(12)	152.90
C14 H14•••O3	0.930	2.528	3.224(11)	131.92

NOTE: All the values are calculated from Platon software[4]

d) Interlayer Distances

Table S8. Interlayer distance in face to face stacking of the crystal structures of **SQIM** determined during VTSXRD experiment from 300 K to 190 K.

Temperature(K)	**Distance (Å)**
190	3.728
250	3.755
300	3.779

NOTE: Interlayer distances were measured between the centres of **SQ** moieties of two successive layers. All the values are calculated from Platon software[4]

Table S9. Interlayer distance in face to face stacking of the crystal structures of **SQIM** determined during VTSXRD experiment from 300K to 450K.

Temperature(K)	**Distance (Å)**
250K	3.758
300K	3.781
350K	3.806
400K	3.827
450K	3.849

NOTE: Interlayer distances were measured between the centres of **SQ** moieties of two successive layers. All the values are calculated from Platon software[4]

Table S10 Interlayer distance in offset stacking in the crystal structures of **SQIM** (Phase-II) determined at150K.

	Distance (Å)
C9 (imidazolium ring)···C1 (squaric acid ring)	3.325(1)
C6 (squaric acid ring)···C14(imidazolium ring)	3.26(1)

Note: There are two **SQ** and two **IM** moieties in the asymmetric unit.

Table S11. Interatomic distances in the imidazolium ring with increasing temperature.

Temperature(K)	**N(2) N(1) (Å)**	**C(5) C(7) (Å)**	**C(6) C(7) (Å)**
250K	2.143(2)	2.188(2)	2.191(1)
300K	2.138(2)	2.182(2)	2.184(2)
350K	2.132(2)	2.172(2)	2.173(2)
400K	2.124(2)	2.160(3)	2.158(3)
450K	2.119(2)	2.152(2)	2.146(2)

NOTE: All the values are calculated from Platon software[4]

8. Thermal expansivity calculated of VTSCXRD experiment for SQIM by PASCal software[5]

Table S12. Thermal expansivity calculated of VTSCXRD experiment from 300K to 190K.

			Directions		
Axes	**α(MK^{-1})**	**σα (MK^{-1})**	**a**	**b**	**c**
X1	-2.7228	0.4932	-0.9609	0.0000	0.2769
X2	2.3742	0.4179	0.0000	1.0000	-0.0000
X3	143.8447	0.4178	0.3007	-0.0000	0.9537
V	143.7998	0.4634			

Table S13. Thermal expansivity calculated of VTSCXRD experiment from 250K to 450K.

			Directions		
Axes	**α(MK^{-1})**	**σα (MK^{-1})**	**a**	**b**	**c**

X1	-14.6781	1.022	0.0000	1.0000	-0.0000
X2	12.6298	3.1128	-0.9526	0.0000	-0.3041
X3	151.1111	0.7976	0.3176	0.0000	0.9438
V	150.0011	2.8526			

9. Thermal Ellipsoids of asymmetric units of SQIM

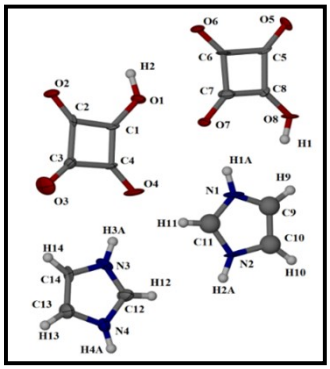

150K (Phase-II)

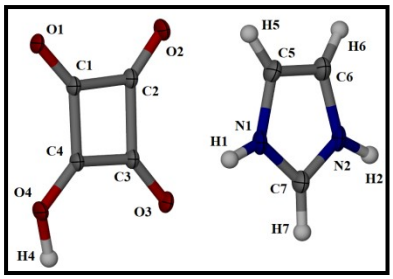

190K

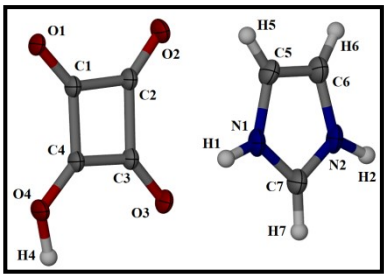

250K

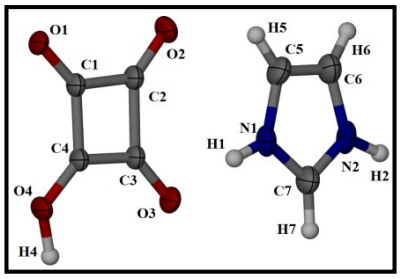

300K

Figure S10 Thermal ellipsoid plots of asymmetric unit of **SQIM** from 150K to 300K with 50% probability by XSeed software[5].

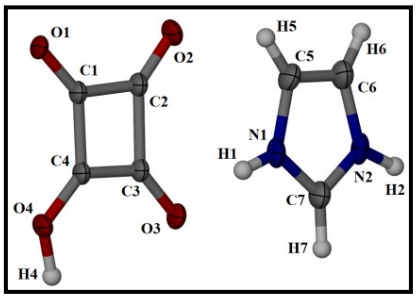

250K

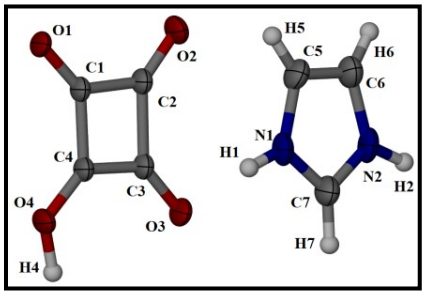

300K

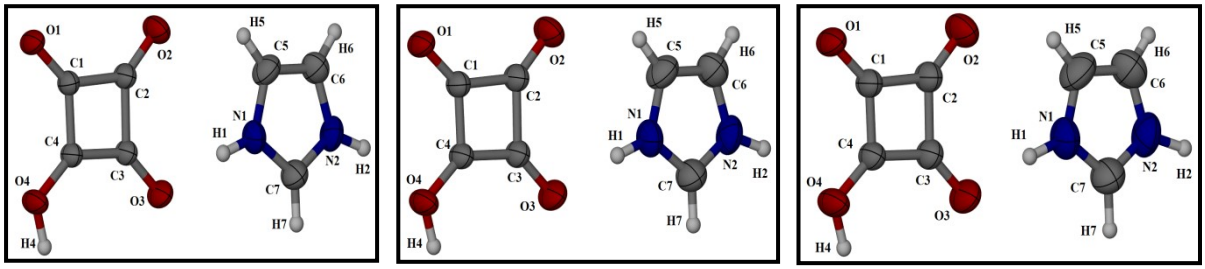

350K **400K** **450K**

Figure S11 Thermal ellipsoid plots of asymmetric unit of **SQIM** from 250K to 450K with 50% probability by XSeed software[6].

10. Diffraction spots of the sheared crystal.

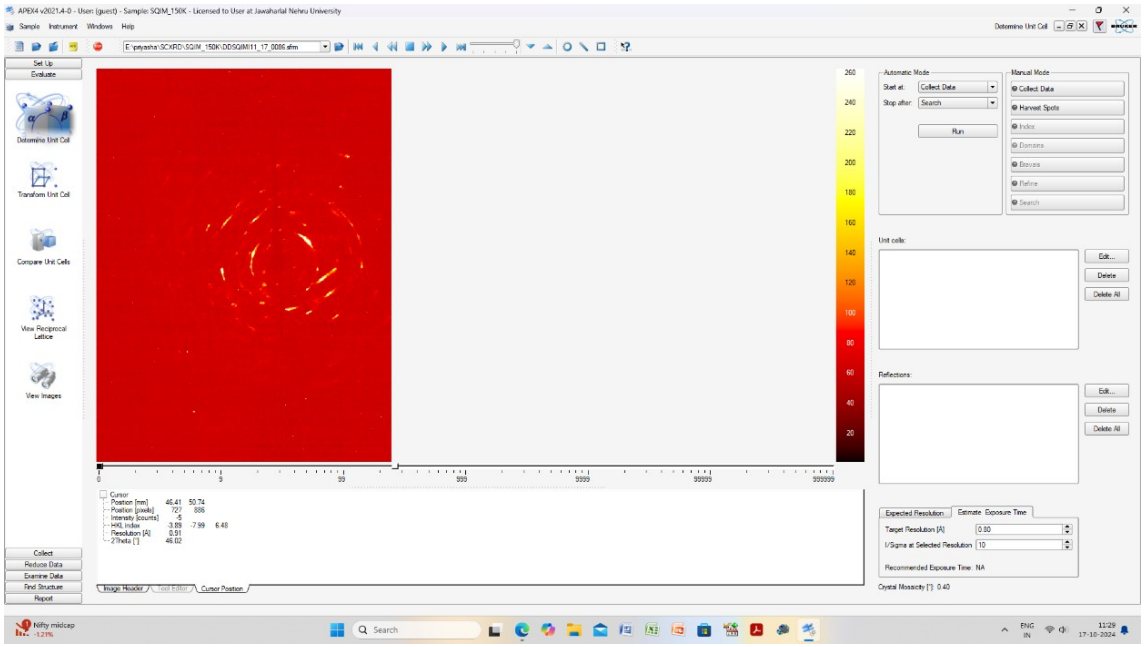

Figure S12 Diffraction spots of sheared crystal observed at 150K during VTSCXRD experiment from RT to Low temperature.

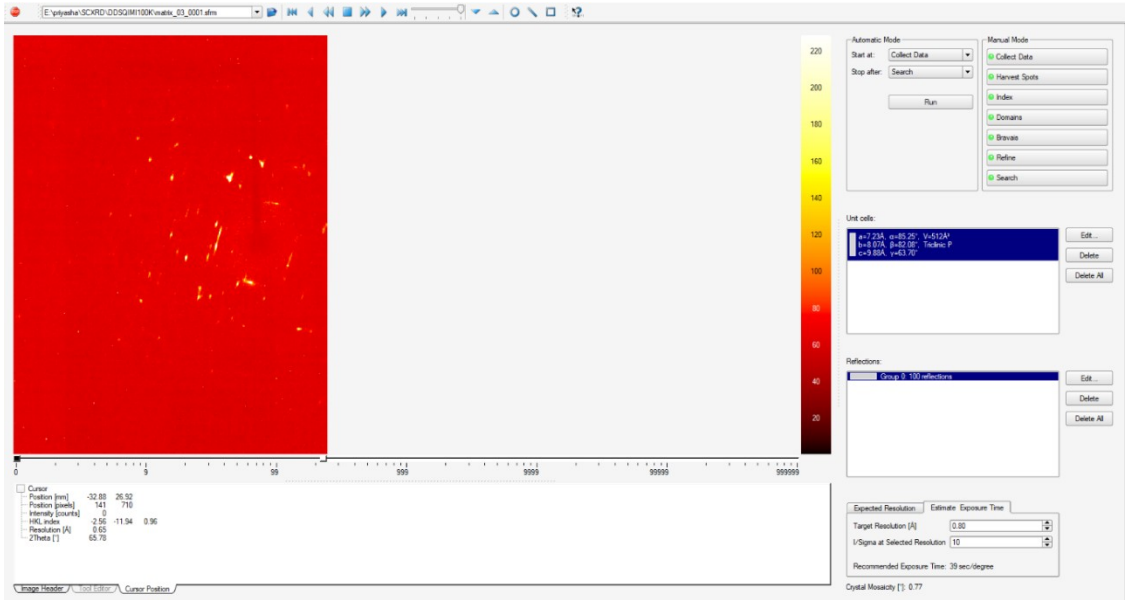

Figure S13 Diffraction spot of the crystal taken from the sheared portion at 100K

11. Description of Videos (Videos S1 and S2)

The jumping behaviour of all the crystals has been recorded by videography to show real-time thermosalient properties. Video S1 shows the jumping of **SQIM,** recorded at low temperature (RT to 193K, Video S2 of **SQIM** shows the jumping observed at high temperature (RT to 403K).

12. References

1. I. L. Karle, D. Ranganathan, and V. Haridas *J. Am. Chem. Soc.,* 1996, 118, 7128
2. SAINT; Bruker AXS Inc., Madison, Wisconsin, USA, **2013.** SADABS; Bruker AXS Inc., Madison, Wisconsin, USA, **2012.**
3. Sheldrick, G. M. SHELXTL v **2014**/5; http//:shelx.uni-ac.gwdg.de/SHELX/index.php.
4. A. L. Spek, *Acta Crystallogr., Sect. D*, 2009, **65**, 148.
5. M. Lertkiattrakul, M. L. Evans, and M. J. Cliffe, *J. open source softw.,* 2023*,* **8***, 5556.*
6. L. J. Barbour, X-Seed. *J. Supramol. Chem.,*2001, **1**, 189.